INTERNATIONAL JOURNAL FOR NUMERICAL METHODS IN FLUIDS, VOL. 16, 525–544 (1993)

EMPLOYMENT OF SECOND-MOMENT CLOSURE FOR CALCULATION OF TURBULENT RECIRCULATING FLOWS IN COMPLEX GEOMETRIES WITH COLLOCATED VARIABLE ARRANGEMENT

BIJAN FARHANIEH, LARS DAVIDSON AND BENGT SUNDÉN

Department of Thermo and Fluid Dynamics, Chalmers University of Technology, 412 96 Göteborg, Sweden

SUMMARY

This paper addresses the implementation of second-moment closure into a collocated variable arrangement body-fitted-finite-volume scheme in which Cartesian velocity components are used. The methods for avoiding instability in the solution procedure are described. A new method for the treatment of the near-wall regions for the momentum equations, as well as the prescription of the stresses at the wall, is described in detail. The performance of the methodology is assessed by applying it to two flow situations, where experimental data are available: the flow over a backward step, and the flow through a sinusoidal pipe constriction. The results are very promising.

KEY WORDS Turbulence modelling Second-moment closure Complex geometries Finite-volume method Collocated variables

INTRODUCTION

The use of a staggered grid in the SIMPLE algorithm has proved the need for storage or recomputation of large amount of geometrical and other quantities. This problem can be avoided by solving the governing equations for the components of the dependent variables in fixed Cartesian co-ordinates on a non-staggered grid. This means that all variables are stored at the centre of the control volume. In this case, when the governing equations are transferred from physical co-ordinates to the computational co-ordinates, the components of the dependent variables can be calculated as scalars. This method has been suggested by Rhie and Chow[1] and has been used by Burns and Wilkes,[2] Majumdar,[3] Peric *et al.*,[4] Miller and Schmidt,[5] Shyy *et al.*,[6] and Braaten and Shyy.[7]

Another advantage of collocated variable arrangement is that the control volume for all variables coincide with the boundaries of the solution field and, therefore, simplifies the specification of the boundary conditions.

However, the use of collocated variable arrangement may cause non-physical oscillations in the pressure and velocity fields. This problem can be overcome by means of the Rhie–Chow[1] interpolation method.

The crucial role of turbulence in most engineering flows necessitates the development and employment of methods which can be used in the simulation of complex turbulent flows with acceptable accuracy. In numerical calculations of turbulent flows, a turbulence model is used to account for the influence of the Reynolds stresses in the time-averaged momentum equations. In

0271–2091/93/060525–20$15.00

Received April 1992
Revised November 1992

many turbulence models, such as the k–ε model, an eddy viscosity assumption is used for calculation of these terms.

The importance of curvature in all recirculating and swirling flows and weakness of the eddy viscosity models to capture the interaction between curvature-related strain and turbulent transport has shifted the attention away from these models and focused on the second-moment closure models (RSM).[8]

The employment of second-moment closure with a general non-orthogonal collocated scheme gives rise to some difficulties. These difficulties are associated with the boundary conditions, the tensorial nature of the wall reflection terms in the pressure–strain components of the Reynolds stress transport equations, numerical instability due to the storage of the calculated stresses in the centre of the control volumes and lack of stability-promoting second-order gradients in the mean flow equations.

The objective of this paper is to describe the use of second-moment closure model in a body-fitted finite-volume code with a collocated variable arrangement.

SOLUTION METHODOLOGY

General calculation procedure

The basic idea in this method is to map the complex flow domain in the physical space to a simple rectangular domain in the computational space by using a curvilinear co-ordinate transformation. In other words, the Cartesian co-ordinate system x_i in the physical domain is replaced by a general non-orthogonal system ξ_i.

The steady transport equation for a general dependent variable Φ in the two-dimensional Cartesian co-ordinates can be written as

$$\frac{\partial}{\partial x_i}(\rho U_i \Phi) = \frac{\partial}{\partial x_i}\left(\Gamma_\Phi \frac{\partial \Phi}{\partial x_i}\right) + S_\Phi, \tag{1}$$

where Γ_Φ is the exchange coefficient and is equal to the viscosity in the momentum equations and to λ/C_p in the energy equation. The dependent variable Φ can be U, V, T, k, ε, $\overline{u_i u_j}$, etc.

The total flux, convective and diffusive fluxes, is defined as

$$I_i = \rho U_i \Phi - \Gamma_\Phi \frac{\partial \Phi}{\partial x_i}. \tag{2}$$

It is now convenient to write equation (1) in the equivalent form

$$\frac{\partial I_i}{\partial x_i} = S_\Phi. \tag{3}$$

Integration of equation (3) over any control volume in the physical space, using Gauss' law, gives

$$\int_A \mathbf{I} \cdot \mathrm{d}\mathbf{A} = \int_V S_\Phi \, \mathrm{d}v. \tag{4}$$

Equation (4) is used for performing the transformation to the computational space co-ordinates (general non-orthogonal co-ordinates) ξ_i.

The scalar advection–diffusion equation (equation (4)) is discretized. The integration of this gives

$$(\mathbf{I} \cdot \mathbf{A})_e + (\mathbf{I} \cdot \mathbf{A})_w + (\mathbf{I} \cdot \mathbf{A})_n + (\mathbf{I} \cdot \mathbf{A})_s = S_\Phi \delta v, \tag{5}$$

where e, w, n and s refer to the faces of the control volume; see Figure 1. The discretized equation is rearranged in the standard form

$$a_P\Phi_P=\sum a_{NB}\Phi_{NB}+S_C, \tag{6}$$

where

$$a_P=\sum a_{NB}-S_P. \tag{7}$$

The index NB refers to the neighbouring nodes. The summation in (6) and (7) is over the neighbouring nodes. The coefficient a_{NB} contain the contribution due to convection and diffusion and the source terms S_P and S_C contain the remaining terms.

Convection. For convenience and simplicity, we restrict ourselves in this and the following subsections only to the east face of the control volume for explanation of the numerical procedure. The total flux **I** contains convective and diffusive fluxes. The first term on the right-hand side of equation (2) is the convective term. The mass flow rate through the east face can be expressed as the scalar product of the velocity and area vectors multiplied by the density. Thus, we have

$$\dot{m}_e=(\rho\mathbf{U}\cdot\mathbf{A})_e=\rho_e(U_eA_{ex}+V_eA_{ey}), \tag{8}$$

where the Cartesian areas are calculated by

$$A_{ex}=|\mathbf{A}|_e\mathbf{n}\cdot\mathbf{e}_x, \qquad A_{ey}=|\mathbf{A}|_e\mathbf{n}\cdot\mathbf{e}_y, \tag{9}$$

where $|\mathbf{A}|_e$ is the total area of the east face, **n** its normal vector and **e** the Cartesian base vector. In order to obtain the velocity components on the control volume faces from those on the control volume centres, the Rhie–Chow[1] interpolation method is used. In this method the weighted linear interpolation in physical space is not used in order to avoid non-physical oscillations in pressure and velocity. The method can be described as follows: Consider the interpolation to the east face of a control volume centred at P in Figure 2. The pressure gradient is subtracted from the velocity components stored at the centre of the control volumes, i.e.

$$\hat{U}_P=U_P-\frac{-(P_e-P_w)\delta v}{|\mathbf{we}|(a_P)_P} \quad \text{and} \quad \hat{U}_E=U_E-\frac{-(P_{ee}-P_e)\delta v}{|\mathbf{e(ee)}|(a_P)_E}. \tag{10}$$

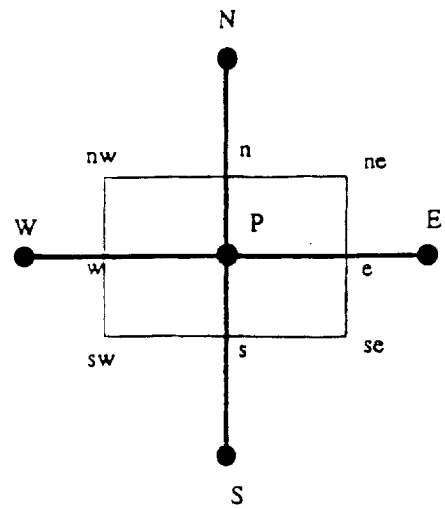

Figure 1. Control volume

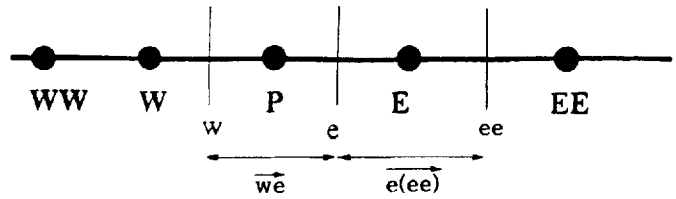

Figure 2. Grid nomenclature

The velocity components on the east face is now calculated as

$$U_e = \Omega_x \hat{U}_E + (1-\Omega_x)\hat{U}_P - \frac{-(P_E - P_P)\delta v}{|\mathbf{PE}|(a_P)_e}, \tag{11}$$

where Ω_x is the interpolation factor in the x-direction and is calculated as

$$\Omega_x = \frac{|\mathbf{Pe}|}{|\mathbf{Pe}| + |\mathbf{eE}|} \tag{12}$$

and P_e, P_w, P_{ee} in equation (10) are calculated by linear interpolation. As seen from equation (11), the pressure gradient is now calculated using the adjacent nodes of the east face. This avoids non-physical oscillations in the pressure field. The velocity V_e is calculated in a similar manner.

Diffusion. The second term in the total flux **I** presented in equation (2) is the diffusion term. Through an area **A**, we have

$$(\mathbf{I}\cdot\mathbf{A})_{\text{diff}} = -\Gamma \mathbf{A}\cdot\nabla\Phi, \tag{13}$$

where $\mathbf{A}\cdot\nabla\Phi$ in equation (13) can, for the east face, be rewritten in Cartesian co-ordinates as

$$(-\mathbf{A}\cdot\nabla\Phi)_e = -\left(A_{ex}\frac{\partial\Phi}{\partial x} + A_{ey}\frac{\partial\Phi}{\partial y}\right)_e \tag{14}$$

and, in general, non-orthogonal co-ordinates as

$$(-\mathbf{A}\cdot\nabla\Phi)_e = -\left(\mathbf{A}\cdot\mathbf{g}_i g^{ij}\frac{\partial\Phi}{\partial\xi_j}\right)_e = -\left(|\mathbf{A}|\mathbf{n}\cdot\mathbf{g}_i g^{ij}\frac{\partial\Phi}{\partial\xi_j}\right)_e, \tag{15}$$

where $\mathbf{g}_i$ is the covariant (tangent) base vector. The appearance of the metric tensor, g^{ij} in equation (15), is due to the fact that the components of the product $\mathbf{A}\cdot\mathbf{g}_i$ and the derivative $\partial\Phi/\partial\xi_j$ are both covariant and the product of their contravariant base vectors is not zero for $i \neq j$ since they are non-orthogonal to each other. The components of g^{ij} can be calculated as shown e.g. in Reference 9.

The normal vector **n** in equation (15) is equal to the cross product of $\mathbf{g}_2$ and $\mathbf{g}_3$ which implies that $\mathbf{n}\cdot\mathbf{g}_3 \equiv \mathbf{n}\cdot\mathbf{g}_2 \equiv 0$. With these identities, equation (15) can be written as

$$(-\mathbf{A}\cdot\nabla\Phi)_e = -\left(|\mathbf{A}|\mathbf{n}\cdot\mathbf{g}_1 g^{1j}\frac{\partial\Phi}{\partial\xi_j}\right)_e. \tag{16}$$

Pressure correction equation. The pressure correction equation is obtained by applying the SIMPLEC algorithm[10] on the non-staggered grid. The mass flux $\dot{m}$ is divided into one old value, $\dot{m}^*$, and another correction value, $\dot{m}'$. The mass flux correction at the east face can be calculated

from

$$\dot{m}'_e=(\rho\mathbf{A}\cdot\mathbf{U}')_e=\rho_e(A_{ex}U'_e+A_{ey}V'_e)=(\rho\mathbf{A}\cdot\mathbf{g}^jU'_j)_e, \tag{17}$$

where U'_j is the covariant correction velocity. The covariant velocity components are related to the pressure gradient[11]

$$U'_j=-\frac{\partial v}{a_P}\frac{\partial P'}{\partial x_j}, \tag{18}$$

where δv is the volume of the control volume. By introducing equation (18) into equation (17), we obtain

$$\dot{m}'=\left[\rho\mathbf{A}\cdot\left(-\frac{\delta v}{a_P}\frac{\partial P'}{\partial x_j}\mathbf{g}^j\right)\right]_e=-\left[\frac{\rho\delta v}{a_P}\mathbf{A}\cdot\nabla P'\right]. \tag{19}$$

Consider the continuity equation in, for simplicity, one dimension:

$$\dot{m}_e-\dot{m}_w=0. \tag{20}$$

If $\dot{m}=\dot{m}^*+\dot{m}'$ and equation (19) are substituted into equation (20), we obtain

$$\left[\frac{\rho\delta v}{a_P}\mathbf{A}\cdot\nabla P'\right]_w-\left[\frac{\rho\delta v}{a_P}\mathbf{A}\cdot\nabla P'\right]_e+\dot{m}^*_e-\dot{m}^*_w=0. \tag{21}$$

This is a diffusion equation for the pressure correction P'. $\mathbf{A}\cdot\nabla p'$ can be calculated from equation (16) by replacing Φ by P'.

Implementation of second-moment closure

The momentum equations for a steady, two-dimensional incompressible flow can be written as

$$\rho U_jU_{i,j}=-P_{,i}+(\mu U_{i,j})_{,j}-(\rho\overline{u_iu_j})_{,j}. \tag{22}$$

Since the time-averaging process generates unknown products, $\rho\overline{u_iu_j}$, the closure variant introduced by Gibson and Launder[12] is used to calculate the Reynolds stresses appearing in the above equation. The model transport equation for the stress components can be expressed as

$$(\rho U_k\overline{u_iu_j})_{,k}=D_{ij}+P_{ij}-\rho\varepsilon_{ij}+\Pi_{ij}, \tag{23}$$

where the terms on the right-hand side represent

P_{ij}: *the production rate of* $\overline{u_iu_j}$,

$$P_{ij}=-\rho\overline{u_iu_l}U_{j,l}-\rho\overline{u_ju_l}U_{i,l}, \tag{24}$$

ε_{ij}: *the dissipation term of* $\overline{u_iu_j}$,

$$\varepsilon_{ij}=2\nu\overline{u_{i,l}u_{j,l}}, \tag{25}$$

D_{ij}: *the turbulent diffusion*,

$$D_{ij}=-\rho\left(\overline{u_iu_ju_l}+\frac{\overline{pu_i}}{\rho}\delta_{jl}+\frac{\overline{pu_j}}{\rho}\delta_{il}\right)_{,l}, \tag{26}$$

Π_{ij}: *the pressure–strain correlation term, which promotes isotropy of turbulence*

$$\Pi_{ij}=\overline{p(u_{i,j}+u_{j,i})}. \tag{27}$$

In order to eliminate the unknown correlations appearing in the Reynolds transport equation, the pressure–strain, dissipation and turbulent diffusion terms require model approximation.

The assumption of local isotropy enables us to approximate the dissipation of $\overline{u_i u_j}$ by

$$\varepsilon_{ij} = \tfrac{2}{3}\delta_{ij}\varepsilon, \tag{28}$$

where ε is the dissipation rate of kinetic energy. The fluctuating pressure p can be eliminated from the pressure–strain correlation via a Poisson equation for p. It can be shown that there are three distinct processes which contribute to the pressure–strain correlation. These are:

1. Interaction of fluctuating velocities $(\Pi_{ij})_1$, which is also referred to as the return-to-isotropy term,[13]

$$(\Pi_{ij})_1 = -\frac{\rho c_1 \varepsilon}{k}\left(\overline{u_i u_j} - \frac{\delta_{ij}}{3}\overline{u_k u_k}\right). \tag{29}$$

2. Interaction of mean strain and fluctuating velocities $(\Pi_{ij})_2$, which is also referred to as the return-to-isotropy of the production term,[14]

$$(\Pi_{ij})_2 = -c_2\left(P_{ij} - \frac{\delta_{ij}}{3}P_{kk}\right). \tag{30}$$

3. Both processes in equations (29) and (30) are influenced by the pressure of wall proximity effects[12] which damp fluctuations normal to the wall and enhance fluctuations parallel to the wall. These effects are presented by

$$(\Pi_{ij})_{w1} = \frac{\rho c_1' \varepsilon}{k}\left[\overline{u_k u_m} n_k n_m \delta_{ij} - \frac{3}{2}\overline{u_k u_i} n_k n_j - \frac{3}{2}\overline{u_k u_j} n_k n_i\right] f, \tag{31}$$

$$(\Pi_{ij})_{w2} = \rho c_2'\left[(\Pi_{km})_2 n_k n_m \delta_{ij} - \frac{3}{2}(\Pi_{ik})_2 n_k n_j - \frac{3}{2}(\Pi_{jk})_2 n_k n_i\right] f, \tag{32}$$

where

$$f = \frac{c_\mu^{0.75} k^{1.5}}{\varepsilon \kappa \Delta\eta}, \tag{33}$$

with $\Delta\eta$ being wall normal distance, f is the wall-distance function and may be related to Cartesian-velocity-oriented components by

$$f_x = n_1^2 f, \qquad f_y = n_2^2 f, \qquad f_{xy} = n_1 n_2 f. \tag{34}$$

The minor contribution of the turbulent diffusion can be approximated by

$$D_{ij} = \left[c_\mu \frac{k^2}{\varepsilon}(\overline{u_i u_j})_{,k}\right]_{,k}. \tag{35}$$

The transport equation (23) for Reynolds stresses are discretized in the same way as for any other dependent variable Φ.

The Reynolds stress equation may be expressed as

$$C_{ij} - D_{ij} = \alpha_{ij,1}P_{11} + \alpha_{ij,2}P_{22} + \alpha_{ij,3}P_{12} + \alpha_{ij,4}P_{kk} + \frac{\rho\varepsilon}{k}(\alpha_{ij,5}\overline{u^2} + \alpha_{ij,6}\overline{v^2} + \alpha_{ij,7}\overline{uv}) + \alpha_{ij,8}\rho\varepsilon, \tag{36}$$

where the commas in the α-coefficients are not the tensorial differential sign. C_{ij} represents the convection term of equation (23). The α-coefficients are tabulated in Table I.

Table I. α-coefficients in equation (36)

	$\overline{u^2}$ $(ii=11)$	$\overline{v^2}$ $(ii=22)$	$\overline{uv}$ $(ii=12)$
$\alpha_{ij,1}$	$1-c_2+2c'_2 f_y$	$-c'_2 f_x$	$1{\cdot}5c'_2 f_{xy}$
$\alpha_{ij,2}$	$-c'_2 f_y$	$1-c_2+2c'_2 f_y$	$1{\cdot}5c'_2 f_{xy}$
$\alpha_{ij,3}$	$c'_2 f_{xy}$	$c'_2 f_{xy}$	$1-c_2+1{\cdot}5c'_2(f_x+f_y)$
$\alpha_{ij,4}$	$\frac{2}{3}(c_2-2c'_2 f_x+c'_2 f_y)$	$\frac{2}{3}(c_2-2c'_2 f_y+c'_2 f_x)$	$-2c'_2 f_{xy}$
$\alpha_{ij,5}$	$-(c_1+2c'_1 f_x)$	$c'_1 f_x$	$-1{\cdot}5c'_1 f_{xy}$
$\alpha_{ij,6}$	$c'_1 f_y$	$-(c_1+2c'_1 f_y)$	$-1{\cdot}5c'_1 f_{xy}$
$\alpha_{ij,7}$	$-c'_1 f_{xy}$	$-c'_1 f_{xy}$	$-(c_1+1{\cdot}5c'_1(f_x+f_y))$
$\alpha_{ij,8}$	$\frac{2}{3}(c_1-1)$	$\frac{2}{3}(c_1-1)$	0

The turbulence energy k and its rate of dissipation ε are calculated by

$$\frac{\partial}{\partial x_i}(\rho U_i k)=\frac{\partial}{\partial x_i}\left[\left(\mu+\frac{\mu_t}{\sigma_k}\right)\frac{\partial k}{\partial x_i}\right]-\rho\varepsilon+\text{Prod.} \tag{37}$$

$$\frac{\partial}{\partial x_i}(\rho U_i \varepsilon)=\frac{\partial}{\partial x_i}\left[\left(\mu+\frac{\mu_t}{\sigma_\varepsilon}\right)\frac{\partial \varepsilon}{\partial x_i}\right]+\frac{\varepsilon}{k}(c_{\varepsilon 1}\,\text{Prod.}-c_{\varepsilon 2}\rho\varepsilon), \tag{38}$$

where the production term, Prod., has the following form in RSM:

$$\text{Prod.}\equiv P_{ij}=-\rho\overline{u_i u_k}\frac{\partial U_j}{\partial x_k}-\rho\overline{u_j u_k}\frac{\partial U_i}{\partial x_k}, \tag{39}$$

whereas in k–ε,

$$\text{Prod.}\equiv P_k=\mu_t\left(\frac{\partial U_i}{\partial x_j}+\frac{\partial U_j}{\partial x_i}\right)\frac{\partial U_i}{\partial x_j}. \tag{40}$$

The model constants are (see e.g. Reference 15)

$$(c_1, c_2, c'_1, c'_2, c_\varepsilon, c_{\varepsilon 1}, c_{\varepsilon 2}, c_\mu)=(1{\cdot}8, 0{\cdot}6, 0{\cdot}5, 0{\cdot}18, 0{\cdot}22, 0{\cdot}18, 1{\cdot}45, 1{\cdot}9, 0{\cdot}09)$$

Stability assurance. At sufficiently high Reynolds number, the viscous effects become negligible and the viscous diffusion term in equation (22) becomes negligible and, in the absence of any linkage between the stresses with their corresponding strain, the problem of numerical instability arises. This problem can be overcome by reformulation of the $\overline{u_i u_j}$-equation in a way that a gradient-type diffusion term $\mu_{ij}U_{l,s}$ appears in the equation. μ_{ij} is called the apparent viscosity[16] and should be unconditionally positive.

The equation for $\overline{u_i u_j}$ at any grid point can be written in the following form:

$$\begin{aligned}a_P\overline{u_i u_j}=&\sum a_{NB}\overline{u_i u_j}_{nb}+\rho\beta_{ij,1}\overline{u^2}\frac{\partial U}{\partial x}+\rho\beta_{ij,2}\overline{v^2}\frac{\partial V}{\partial y}+\rho\beta_{ij,3}\overline{v^2}\frac{\partial U}{\partial y}+\rho\beta_{ij,4}\overline{u^2}\frac{\partial V}{\partial x}+\rho\beta_{ij,5}\overline{uv}\frac{\partial u}{\partial x}\\&+\rho\beta_{ij,6}\overline{uv}\frac{\partial V}{\partial y}+\rho\beta_{ij,7}\overline{uv}\frac{\partial U}{\partial y}+\rho\beta_{ij,8}\overline{uv}\frac{\partial V}{\partial x}\\&+\frac{\varepsilon}{k}(\rho\beta_{ij,9}\overline{u^2}+\rho\beta_{ij,10}\overline{v^2}+\rho\beta_{ij,11}\overline{uv})+\beta_{ij,12}\rho\varepsilon.\end{aligned} \tag{41}$$

The β-coefficients are tabulated in Table II. Note that the comma in the β-coefficients are not the tensorial differential sign.

The apparent viscosities extracted from the above equation are

$$\hat{\mu}_{ii}=\frac{\rho\beta_{ii,\,i}\overline{u_i^2}}{a_{pii}+\rho\beta_{ii,\,(i+8)4\varepsilon/k}} \quad \text{(no summation on } i\text{)}, \tag{42}$$

$$\hat{\mu}_{ij}=\frac{\beta_{ij,\,(i+2)}\overline{u^2}^{(3-i)}}{a_{pij}+\beta_{ij,\,11\varepsilon/k}} \quad (i\neq j \text{ and no summation on } i \text{ and } j). \tag{43}$$

Insertion of these viscosities into the U-momentum equation, for example, gives in Cartesian co-ordinates,

$$\rho(UU_j)_{,\,j}=-P_{,\,1}+(\mu_{11}U_{1,\,1})_{,\,1}+(\mu_{12}U_{1,\,2})_{,\,2}+S_{\text{extra}}. \tag{44}$$

The remaining terms in equation (41) after extraction of apparent viscosities are inserted into S_{extra}.

According to equation (16), the apparent viscosities should be transferred to the general non-orthogonal co-ordinates (ξ, η).

The rules for transformation from the Cartesian co-ordinate system to any other general co-ordinate system and vice versa are

$$\left[\frac{\partial\phi}{\partial\xi_i}\right]=[A]\left[\frac{\partial\phi}{\partial x_i}\right], \tag{45}$$

$$\left[\frac{\partial\phi}{\partial x_i}\right]=\frac{[B]}{J}\left[\frac{\partial\phi}{\partial\xi_i}\right], \tag{46}$$

where $[A]$ and $[B]$ are given in Reference 17. J (=Jacobian) is the determinant of $[A]$, which is equal to $\sqrt{g}$, see Reference 9. The derivatives $\partial U/\partial x$ and $\partial V/\partial x$, for example, can be written by

Table II. β-coefficients in equation (41)

	$\overline{u^2}$ $(ii=11)$	$\overline{v^2}$ $(ii=22)$	$\overline{uv}$ $(ii=12)$
$\beta_{ij,\,1}$	$2-\frac{4}{3}c_2+\frac{2}{3}c'_2(4f_x+f_y)$	$\frac{2}{3}c_2-\frac{4}{3}c'_2(f_x+f_y)$	c'_2f_{xy}
$\beta_{ij,\,2}$	$\frac{2}{3}c_2-\frac{4}{3}c'_2(f_x+f_y)$	$2-\frac{4}{3}c_2+\frac{2}{3}c'_2(f_x+4f_y)$	c'_2f_{xy}
$\beta_{ij,\,3}$	c'_2f_{xy}	c'_2f_{xy}	$1-c_2+\frac{3}{2}c'_2(f_x+f_y)$
$\beta_{ij,\,4}$	c'_2f_{xy}	c'_2f_{xy}	$1-c_2+\frac{3}{2}c'_2(f_x+f_y)$
$\beta_{ij,\,5}$	c'_2f_{xy}	c'_2f_{xy}	$1-c_2+\frac{3}{2}c'_2(f_x+f_y)$
$\beta_{ij,\,6}$	c'_2f_{xy}	c'_2f_{xy}	$1-c_2+\frac{3}{2}c'_2(f_x+f_y)$
$\beta_{ij,\,7}$	$2-\frac{4}{3}c_2+\frac{2}{3}c'_2(4f_x+f_y)$	$\frac{2}{3}c_2-\frac{4}{3}c'_2(f_x+f_y)$	c'_2f_{xy}
$\beta_{ij,\,8}$	$\frac{2}{3}c_2-\frac{4}{3}c'_2(f_x+f_y)$	$2-\frac{4}{3}c_2+\frac{2}{3}c'_2(f_x+4f_y)$	c'_2f_{xy}
$\beta_{ij,\,9}$	$c_1+2c'_1f_x$	$-c'_1f_x$	$\frac{3}{2}c'_1f_{xy}$
$\beta_{ij,\,10}$	$-c'_1f_y$	$c_1+2c'_1f_y$	$\frac{3}{2}c'_1f_{xy}$
$\beta_{ij,\,11}$	c'_1f_{xy}	c'_1f_{xy}	$c_1+\frac{3}{2}c'_1(f_x+f_y)$
$\beta_{ij,\,12}$	$\frac{2}{3}(1-c_1)$	$\frac{2}{3}(1-c_1)$	0

means of equation (46) as

$$\frac{\partial U}{\partial x}=\frac{B_{11}}{J}\frac{\partial U}{\partial \xi}+\frac{B_{12}}{J}\frac{\partial U}{\partial \eta},$$

$$\frac{\partial U}{\partial y}=\frac{B_{21}}{J}\frac{\partial U}{\partial \xi}+\frac{B_{22}}{J}\frac{\partial U}{\partial \eta}. \tag{47}$$

Identification of equations (42), (43) and (47) gives the apparent viscosities in general orthogonal co-ordinates as

$$\mu_{11}=\hat{\mu}_{11}(B_{11})^2+\hat{\mu}_{12}(B_{21})^2, \tag{48}$$

$$\mu_{12}=\hat{\mu}_{11}(B_{12})^2+\hat{\mu}_{12}(B_{22})^2, \tag{49}$$

where μ_{11} and μ_{12} are associated with $\partial U/\partial\xi$ and $\partial U/\partial\eta$, respectively, neglecting the terms containing cross-derivatives. Above, the integrated diffusion term (i.e. the first derivatives) has been transformed.

Due to the involvement of the normal stresses in the apparent viscosities, special care must be taken to assure that at no stage in the iterative sequence do the normal stresses become negative. This can be assured by special treatment of the source term

$$S=S_C+S_P\overline{u_i^2}. \tag{50}$$

If the production terms during the iteration process attain positive values, they are insered into the constant part of the source term S_C; otherwise, they are inserted into S_P:

$$S_C=\max(\alpha_{ii,1}P_{11},0)+\max(\alpha_{ii,2}P_{22},0)$$
$$+\max(\alpha_{ii,3}P_{12},0)+\max(\alpha_{ii,4}P_{kk},0)+\frac{\varepsilon}{k}\alpha_{ii,(7-i)}\overline{u_{3-i}^2}+\alpha_{ii,8}\varepsilon, \tag{51}$$

$$S_P=[\min(\alpha_{ii,1}P_{11},0)+\min(\alpha_{ii,2}P_{22},0)$$
$$+\min(\alpha_{ii,3}P_{12},0)+\min(\alpha_{ii,4}P_{kk},0)]/\overline{u_i^2}+\alpha_{ii,(4+i)}\frac{\varepsilon}{k}. \tag{52}$$

Boundary conditions

Inlet and outlet. In the present case studies the fully developed values of all the variables are prescribed at the inlet. Since there are no area changes (in our cases) at the outlet region, and this region is sufficiently long and far downstream, the flow may safely be assumed as fully developed, which implies negligible streamwise gradients of all variables

$$\frac{\partial\Phi}{\partial x}=0, \quad \Phi=U_i, P', k, \varepsilon, \overline{u_iu_j}. \tag{53}$$

Walls. Due to the viscous influences near the walls, the local Reynolds number becomes very small; thus, the turbulence model, which is appropriate only for high Reynolds numbers, becomes inadequate. Both this fact and the steep variation of the properties near the walls necessitate a special treatment for nodes close to the walls.

When using wall functions for the momentum equations, shear stresses are prescribed at the boundaries. In Cartesian geometries or when solving for covariant velocity components where the velocity components are parallel to the boundaries this poses no problem. The procedure of applying shear stresses in a general co-ordinate system when the velocity components are not

parallel to the boundaries is more complicated. In the present work a novel, simple treatment is proposed.

The wall function employed in this work can be summarized as follows:

(a) *For* $\eta^+ \geq 11{\cdot}63$, *where* $\mu_t/\mu \gg 1$, $\tau \approx \tau_w$:

1. The wall shear stress is obtained by calculating the viscosity at the node adjacent to the wall from the log law. The turbulent viscosity used in the momentum equations is prescribed at the nodes adjacent to the wall as follows:

$$\tau_w = \rho U_*^2 = \mu_t \frac{\partial U}{\partial \eta} \approx \mu_t \frac{U}{\eta}. \tag{54}$$

For μ_t, we obtain

$$\mu_t = \frac{U_*}{U} \rho U_* \eta. \tag{55}$$

The law of the wall can be written as

$$\frac{U}{U_*} = \frac{1}{\kappa} \ln(E\eta^+). \tag{56}$$

Finally, we have for μ_t

$$\mu_t = \frac{\rho U_* \eta \kappa}{\ln(E\eta^+)}, \tag{57}$$

where $E = 9$ and the von Karman constant, $\kappa = 0{\cdot}41$. η denotes the normal distance to the wall.

2. The turbulent kinetic energy is set as

$$k = c_\mu^{-0{\cdot}5} U_*^2. \tag{58}$$

3. The energy dissipation rate is set as

$$\varepsilon = \frac{U_*^3}{\kappa \eta}. \tag{59}$$

4. The turbulent stresses are obtained by two methods (BC1 and BC2 below)

(i) The first method (BC1) was derived by Launder *et al.*,[18] who studied several well-documented wall flows and presented the following boundary conditions for the turbulent stresses:

$$\overline{uv} = -U_*^2 + y \frac{\partial p}{\partial x}, \tag{60}$$

$$\overline{u^2} = 5{\cdot}1 U_*^2, \tag{61}$$

$$\overline{v^2} = 1{\cdot}0 U_*^2, \tag{62}$$

$$\overline{w^2} = 2{\cdot}3 U_*^2, \tag{63}$$

(ii) The second method (BC2) has been presented by Lein and Leschziner.[19] They derived the following values of the stresses in the log-law region by applying the stress equation to local energy equilibrium, and setting the wall distance function equal to unity and

using equation (59):

$$\hat{\overline{u^2}} = 1{\cdot}098k, \tag{64}$$

$$\hat{\overline{v^2}} = 0{\cdot}247k, \tag{65}$$

$$\hat{\overline{uv}} = 0{\cdot}255k, \tag{66}$$

$$\hat{\overline{w^2}} = 0{\cdot}653k, \tag{67}$$

The above stresses are wall-oriented and should be transformed to the Cartesian co-ordinate system in which the velocity components are prescribed within the numerical scheme. We then have

$$\overline{u^2} = \hat{\overline{u^2}} t_1^2 + \hat{\overline{v^2}} n_1^2 + 2\hat{\overline{uv}} t_1 n_1, \tag{68}$$

$$\overline{u^2} = \hat{\overline{u^2}} t_2^2 + \hat{\overline{v^2}} n_2^2 + 2\hat{\overline{uv}} t_2 n_2, \tag{69}$$

$$\overline{uv} = \hat{\overline{u^2}} t_1 t_2 + \hat{\overline{v^2}} n_1 n_2 + \hat{\overline{uv}}(t_1 n_2 + t_2 n_1), \tag{70}$$

where t_1, t_2, n_1 and n_2 are the tangential and normal components of the wall-oriented unit vector, respectively.

(b) *For* $\eta^+ \leq 11{\cdot}63$, *where* $\mu_t/\mu \ll 1$, $\tau \approx \tau_w$, U_* *is obtained from*

$$\frac{U}{U_*} = \frac{U_* \eta}{\nu}. \tag{71}$$

Numerical solution procedure

A finite-volume method with collocated variable arrangement is used for solving the equation system. The pressure and mean velocity fields are coupled by the SIMPLEC algorithm.[10] The diffusive terms are discretized with the central differencing scheme. Three different discretization schemes have been tested for the convective terms: hybrid upwind/central difference,[11] the second-order scheme of van Leer[20] and quadratic upstream-weighted interpolation scheme of Leonard.[21] The algebraic equation system arising from the discretization is solved by the TDMA algorithm. The convergence criterion is that the sum of the absolute residuals divided by the inlet fluxes is below 10^{-5} for all variables. This criterion was satisfied for all results presented in this paper.

RESULTS AND DISCUSSION

The performance of the above-described methodology is assessed by comparing computations with experiments and other numerical calculations in two examples: the flow behind a backward-facing step[22] and the flow through a sinusoidal pipe constriction.[23]

The first test case—backward-facing step

The schematic diagram of this case is shown in Figure 3. At the inlet, which is located at $5H$ upstream of the step, the fully developed values of the dependent variables are imposed. The computations were carried out for 100×38 and 80×30 grid points. No significant differences were observed in the results. However, in order to compare the obtained results with the

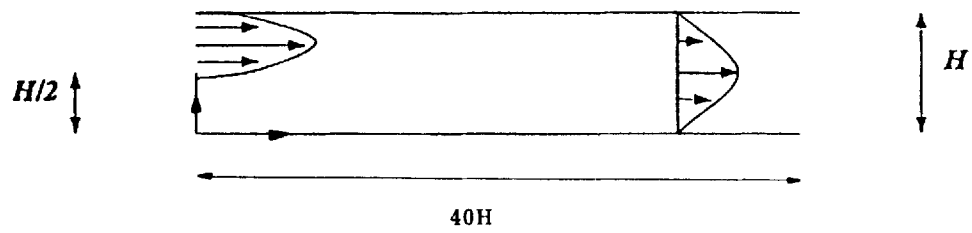

Figure 3. Backward-facing step configuration

numerical results calculated by others,[15] 100 × 38 grid points were chosen. Turbulent stresses and velocity distributions at three different axial locations using the RSM and k–ε models are presented in Figures 4 and 5. These results are compared with the experimental data of Durst and Schmitt[21] and the numerical results obtained by Obi *et al.*[15] The reattachment point is predicted to be at $x/H = 7{\cdot}908$ and $x/H = 7{\cdot}397$ using the RSM and k–ε models, respectively. The experimental reattachment length is 8·5. From the velocity profiles, it can be seen that the k–ε model is more diffusive than the RSM, and that the velocity gradient in the shear layer bounding the recirculation region is smeared out when the k–ε model is used; see Figure 4. The reason for this is that turbulence is stabilized (damped) by the convex streamlines. The RSM does account for this phenomena, whereas the k–ε model does not. However, both models underpredict the strength of the back flow; see Figure 4. This is further confirmed by comparing the shear stresses in Figure 5(a), where the experimentally measured $\overline{uv}$ are very small—compared to the predicted shear stresses—in the backflow region. One explanation for the discrepancy can be the large scale, highly turbulent structure of the separated, recirculating flow, where the turbulent fluctuations are of the same order as the mean velocities.[24, 25] The predicted $\overline{u^2}$-values are rather well in agreement with the experimental data. It is interesting to note that, as the reattachment point is approached, the difference between the experimental $\overline{u^2}$ and $\overline{v^2}$ decreases, i.e. the anisotropy in the

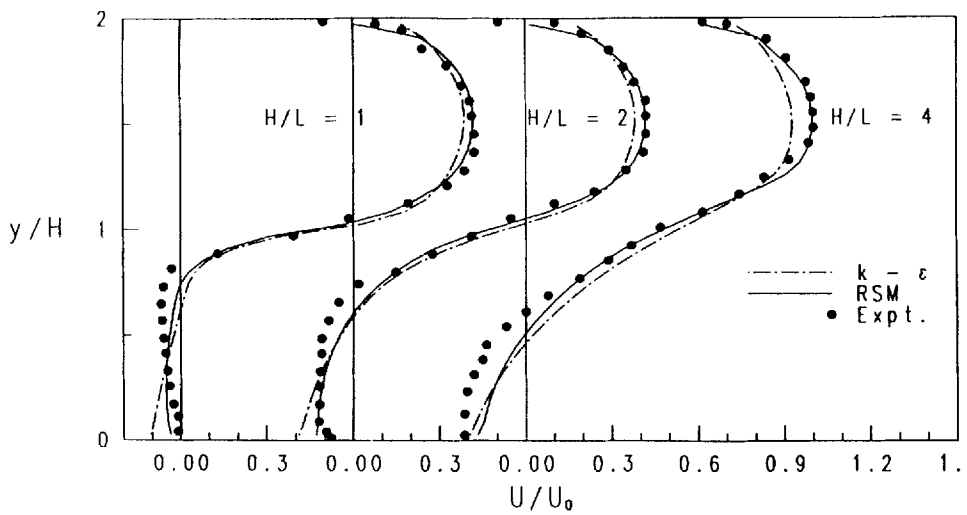

Figure 4. Mean velocity profiles calculated with two different turbulence models

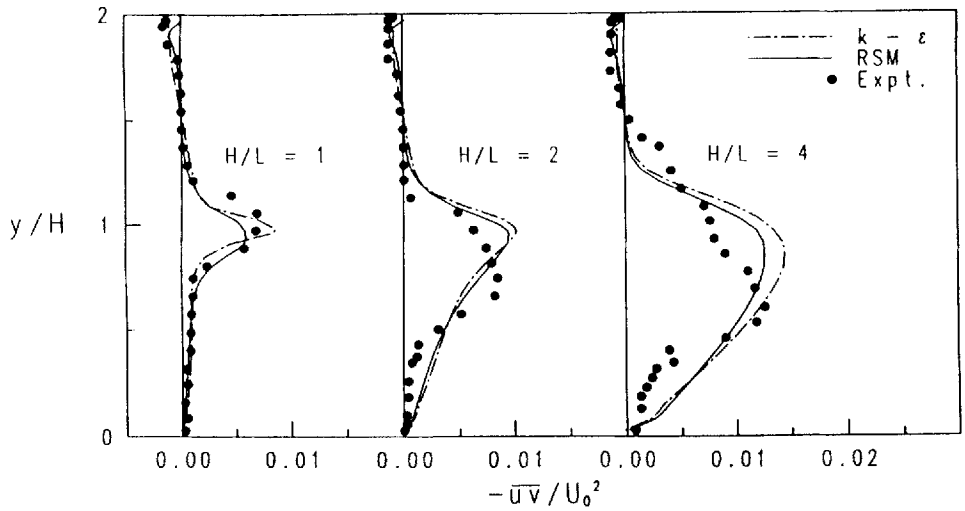

Figure 5(a). Turbulent shear stress calculated with two different turbulent models

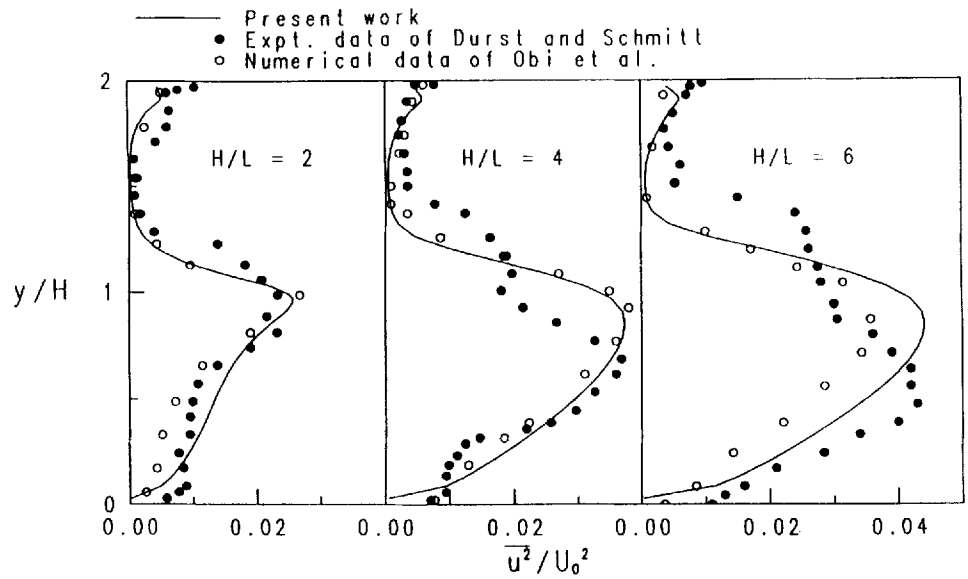

Figure 5(b). Comparison of the $\overline{u^2}$-component of normal stresses in recirculating region with experimental and numerical data

experimental normal stresses decreases; this is not the case in the RSM calculations; see Figures 5(b) and 5(c). These observed differences can be a combination of two effects. First, the near-wall terms $(\Pi_{ij})_{w1}$ and $(\Pi_{ij})_{w2}$ (see equations (31) and (32)) in the RSM are not suitable for stagnation-like flow in the reattachment region. However, there are no better methods to take into account the effects of walls on turbulence. Second, the experimental flow in this region is highly unsteady

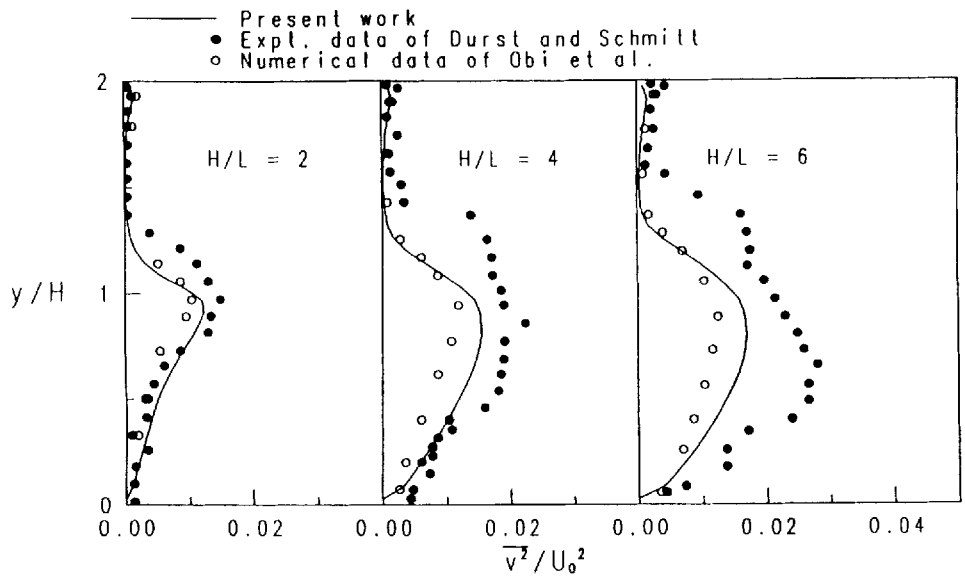

Figure 5(c). Comparison of the $\overline{v^2}$-component of normal stresses in recirculating region with experimental and numerical data

with large fluctuations which are greater than or at least comparable to the mean backflow velocities.[23] Thompson and Whitelaw[24] conjecture that positive instantaneous velocities were measured for at least part of the time at all locations throughout this region. The unsteadiness of the flow in this region is likely to reduce the anisotropy.

As seen, near the step, the computational data of the present work are in good agreement with the experimental data. However, further downstream, the agreement becomes worse. As seen from Figure 5(c), the normal stress $\overline{v^2}$ is underpredicted compared to $\overline{u^2}$ and $\overline{uv}$. The calculations presented by Obi *et al.*[15] underpredict $\overline{v^2}$ even more. However, when they restricted the effect of the wall reflection (equation (31) and (32)) terms to the near-wall region $y^+ \leq 100$, the results of $\overline{v^2}$ improved significantly. In the present work, the effect of the wall reflection terms is taken fully into account throughout this case.

The calculations were performed by discretizing the convection terms of the turbulent quantities by the hybrid scheme. The convection terms of the momentum equations were approximated by the hybrid as well as the van Leer scheme. No changes in the results could be observed when either of the schemes was used, indicating limited numerical diffusion.

The second test case—sinusoidal pipe constriction

The schematic diagram of the stenosis is depicted in Figure 6. To assess the effect of curvature of the grid lines on the performance of the code in simulating the turbulent flows in geometries with curvilinear boundaries, the turbulent flow through an axisymmetric constriction in a tube is studied using both a RSM and a k–ε model. To study the grid size effects on numerical accuracy, exploratory test runs were carried out for three different grid sizes. The results are compared with the experimental data obtained by Deshpande *et al.*;[19] see Figure 7. The results are only slightly affected by the grid size. As in the previous case, 100×36 grid points were chosen for the final

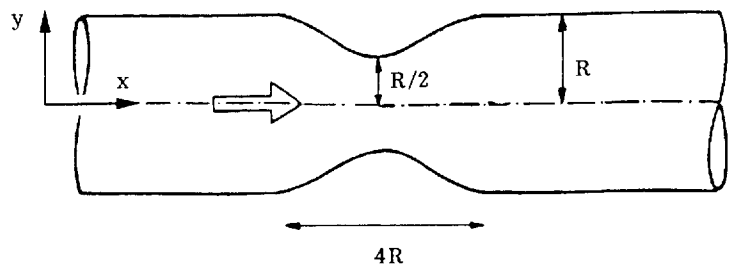

Figure 6. Schematic diagram of the pipe with constriction

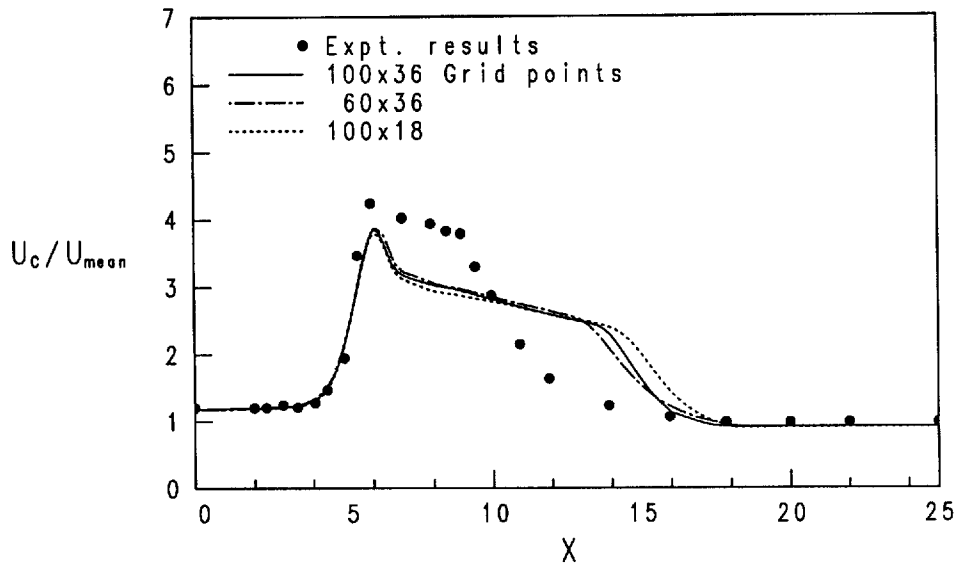

Figure 7. Centreline velocity distribution in the pipe with constriction for different mesh sizes

computations. In the computations two different wall boundary condition methods, described previously, are applied for prescribing the Reynolds stresses. The second boundary condition (BC2) gives slightly better results compared to (BC1). Therefore, the computations were performed by adopting (BC2). The convection terms of the momentum equations were approximated by three different schemes, i.e. hybrid, van Leer and QUICK schemes. The convection terms of turbulence quantities were discretized by the hybrid scheme only in order to avoid convergence problems. The comparison of these three schemes are presented in Figure 8. The centreline velocity predicted by the various scheme for the RSM is not extremely different. However, the k–ε model with the van Leer scheme gives results differing considerably from the other schemes. Lein and Leschziner[19] adopted a combination of QUICK and MUSCL for approximation of convection of momentum and turbulence quantities, respectively. The results obtained in Reference 19 are almost identical to the ones in the present work, where the van Leer and QUICK schemes are used.

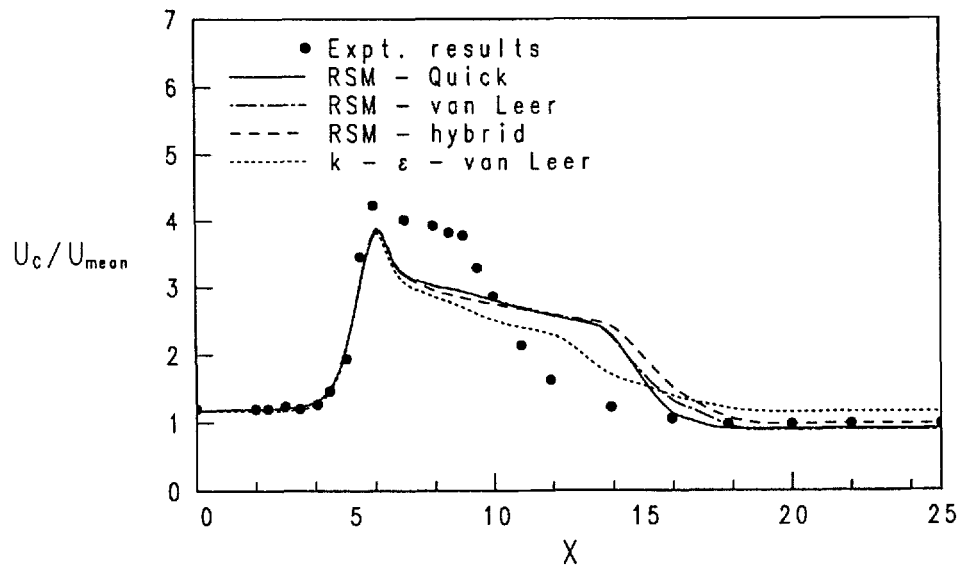

Figure 8. Comparison of the centreline velocity distribution calculated with three different schemes

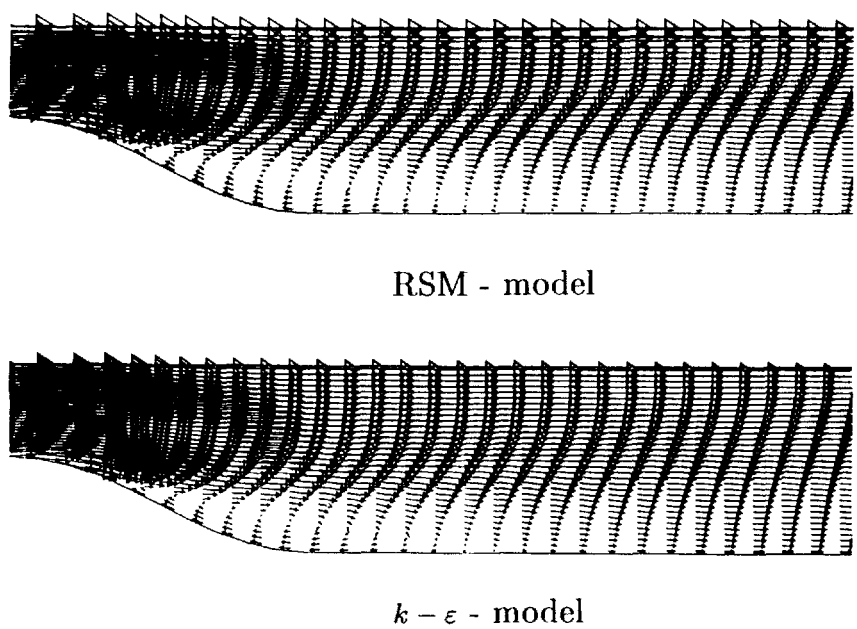

Figure 9. Velocity vectors at the downstream of the throat calculated by two different turbulence models

The velocity vectors and streamfunction are plotted and presented in Figures 9 and 10. This case presents a region of strong acceleration with a converging section and a region of severe adverse pressure gradient which results in flow separation. Both models, k–ε and the stress closure, predict the presence of a recirculating region. As seen from Figures 9 and 10, the

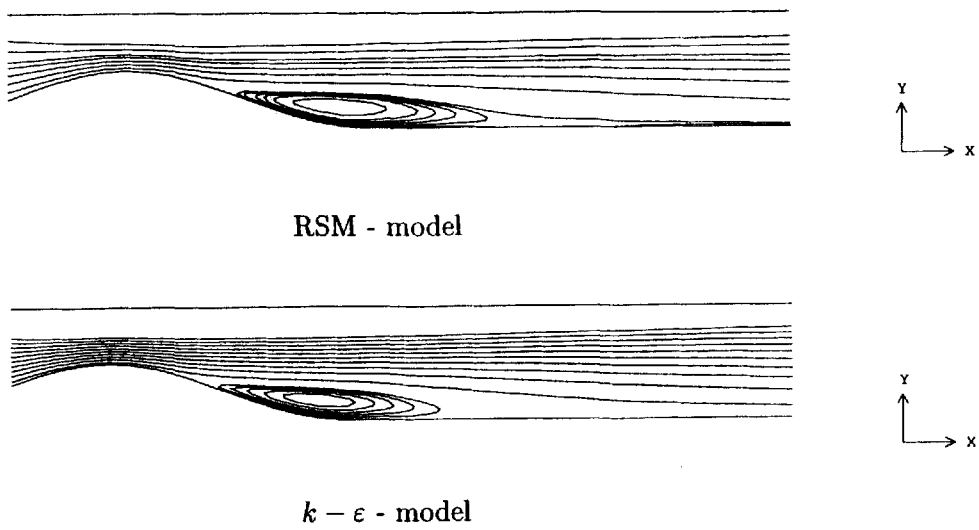

Figure 10. Streamfunction contours in the pipe with constriction—calculated with two different turbulence models

second-moment closure predicts a longer and higher recirculation zone than the k–ε model. Figure 9 shows that the second-moment closure predicts a thicker, wider and higher shear layer bordering the recirculating region. This can probably be attributed to the ability of the RSM to account for streamline curvature. In the shear layer enclosing the recirculating region, the streamlines have convex curvature, which stabilizes the turbulence. Another reason why the k–ε model produces more turbulence than the RSM is that the contraction region causes negative production of $\overline{u^2}$, a phenomenon which RSM accounts for, but the k–ε model does not. The production terms due to the $\partial U/\partial x$ derivative in the two models are:

$$\text{RSM:} \quad P_{11} = -2\rho\overline{u^2}\frac{\partial U}{\partial x}, \tag{72}$$

$$k\text{–}\varepsilon\text{:} \quad P_k = \mu_t\left(\frac{\partial U}{\partial x}\right)^2. \tag{73}$$

The production term P_k in the k–ε model can never become negative in accelerating flow, but the RSM faithfully reproduces the physical situation.

Axial variations of the centreline velocity in Figure 8 show good agreement with the experimental data up to the throat section. A difference can be observed beyond this point. None of the models predicts the correct behaviour of the centreline velocity, but the second closure model responds more sensitively to the adverse pressure gradient beyond the throat; see Figure 8. As mentioned above, both models predict the recirculating region. However, this region is found to be thinner and longer than the region which actually exists. Comparing the prediction of the models, it seems that the stress model captures the recirculation somewhat better than the k–ε model. The computed and the experimental data reach a good agreement far downstream since both tend to fully developed values.

Unlike the previous case, the wall reflection terms caused some difficulties in this case. By taking these terms into account, it was observed that the recirculating region stretched along the axial direction near the wall. The main purpose of these terms is to damp the wall-normal

components as a function of the turbulent length scale and the wall distance. In this case, where a separated shear layer associated with large turbulent length scales develops from the throat, this effect becomes unfavourably strong in the core of the pipe flow despite the large distances from the wall. Therefore, the computations were performed without applying wall reflection terms in the recirculating region. Other works have reported similar problems.[21]

It is somewhat disappointing that the RSM does not produce results in much closer agreement than the k–ε model does. One reason for the poor performance of the RSM can be due to inadequate modelling of the near-wall region; the near-wall correction term in $\overline{v^2}$ is one problem. Another one might be due to the wall functions.

CONCLUSIONS

The successful incorporation of the Reynolds stress closure into a body-fitted-finite-volume framework in which collocated variable arrangement as well as Cartesian velocity components are used is reported in this paper. The absence of diffusion-related strain terms in the momentum equations at high Reynolds numbers causes instability in the solution sequence. This problem and the problem of the appearance of non-physical oscillations in the solution domain due to the employment of collocated variable arrangement are addressed in detail. The near-wall treatment of the dependent variables, necessary to match the curvilinear boundaries is also presented. Two complex applications were used to assess the performance of the described methodology. The computed data of flow over a backward-facing step are in good agreement with the experimental results in the vicinity of the step. However, further downstream, discrepancies can be observed. The calculated results of the flow through a pipe constriction show the correct prediction of the recirculating zone. The predictions of the velocity along the axis of the pipe agree reasonably well with the experimental data. However, both turbulence models fail in predicting the axial velocity variation in the diverging section of the pipe.

APPENDIX: NOMENCLATURE

A	area
a	coefficients in discretized equations
$c_1, c_2, c'_1, c'_2,$ $c_\varepsilon, c_{\varepsilon 1}, c_{\varepsilon 2},$ c_μ	coefficients in the turbulence models
D_{ij}	turbulent diffusion term
$\mathbf{e}_i$	Cartesian unit base vector
f	wall-distance function
g_{ij}, g^{ij}	covariant and contravariant components of the metric tensor
$\mathbf{g}_i$	covariant base vector (=unit base vector tangential to the grid lines)
g	determinant of g_{ij}
H	inlet height of the backward-facing step
$\mathbf{I}$	total flux (convective and diffusive fluxes)
k	turbulent kinetic energy
L	length of the backward-facing step
$\dot{m}$	mass flow rate
$\mathbf{n}$	unit normal vector
P	pressure
P'	pressure correction

P_k	production term in k–ε model
P_{ij}	production term in RSM
S_Φ	source term in general equation
T	temperature
u	fluctuation velocity in the main flow direction
U	velocity in x-direction
U_c	centreline velocity in x-direction
U_i	velocity components
U_{mean}	mean velocity
V	velocity in y-direction
v	fluctuation velocity in y-direction
x	streamwise co-ordinate
y	transversal co-ordinate
δv	volume of a control volume
ε	dissipation rate of the turbulent kinetic energy
ε_{ij}	dissipation term of $\overline{u_i u_j}$
η	distance normal to the wall
λ	thermal conductivity
μ	dynamic viscosity
ν	kinematic viscosity
ξ_i	co-ordinates along (tangential to) the grid lines
Π_{ij}	pressure–strain correlation term
ρ	density
Φ	general dependent variable
$-\rho\overline{u_i u_j}$	Reynolds stress components
Ω	interpolation factor

REFERENCES

1. C. M. Rhie and W. L. Chow, 'Numerical study of the turbulent flow past an airfoil with trailing edge separation', *AIAA J.*, **2**, 1527–1532 (1983).
2. A. D. Burns and N. S. Wilkes, 'A finite difference method for the computation of fluid flow in complex three-dimensional geometries', *AERE R 12342*, Harwell Laboratory, U.K., 1986.
3. S. Majumdar, 'Developing of a finite-volume procedure for prediction of fluid flow problems with complex irregular boundaries, *SFB 210/T/29*, University of Karlsruhe, 1986.
4. M. Peric, R. Kessler and G. Scheuerer, 'Comparison of finite-volume numerical methods with staggered and collocated grids', *Comput. Fluids*, **16**, 389–403 (1988).
5. T. F. Miller and F. W. Schmidt, 'Use of a pressure-weighted interpolation method for the solution of the incompressible Navier–Stokes equations on a non-staggered system', *Numer. Heat Transfer*, **14**, 213–233 (1988).
6. W. Shyy, S. S. Tong and S. M. Corre, 'Numerical recirculating flow calculation using body-fitted coordinate system', *Numer. Heat Transfer*, **8**, 99–113 (1985).
7. M. Braaten and W. Shyy, 'Study of recirculating flow computation using body-fitted coordinates: consistency aspects and mesh skewness', *Numer. Heat Transfer*, **9**, 559–574 (1986).
8. M. A. Leschziner, 'Modelling engineering flows with Reynolds stress turbulence closure', *J. Wind Eng. Ind. Aerodynam.*, **35**, 21–47 (1990).
9. F. Irgens, *Tensoranalyse og Kontinumsmekanik, del III*, Institutt for Mekanikk, Norge Tekniska Hoskole, Trondheim 1966 (in Norwegian).
10. J. P. Van Doormal and G. D. Raithby, 'Enhancements of the SIMPLE method for predicting incompressible fluid flows', *Numer. Heat Transfer*, **7**, 147–163 (1984).
11. S. V. Patankar, 'Numerical Heat Transfer and Fluid Flow, McGraw-Hill, Washington, DC, 1980.
12. M. M. Gibson and B. E. Launder, 'Ground effects on pressure fluctuations in the atmospheric boundary layer', *J. Fluid Mech.*, **86**, 491 (1978).
13. J. C. Rotta, Turbulente Strömungen, B. G. Teubner, Stuttgart, 1972.

14. D. Naot, A. Shavit and M. Wolfshtein, 'Interaction between components of the turbulent-velocity correlation tensor', *Israel J. Techn.*, **8**, 259 (1970).
15. S. Obi, M. Perić and G. Scheuerer, 'A finite-volume calculation procedure for turbulent flows with second-order closure and collocated variable arrangement', *Proc. 7th Symp. Turbulent Shear Flows*, Stanford University, 1989, pp. 17.4.1–17.4.6.
16. P. G. Huang and M. A. Leschziner, 'Stabilization of recirculating-flow computations performed with second moment closures and third-order discretization', *Proc. 5th Symp. Turbulent Shear Flows*, Cornell University, 1985, pp. 20.7–20.12.
17. L. Davidson and B. Farhanieh, 'CALC-BFC: a finite-volume code employing collocated variable arrangement and Cartesian velocity components for computation of heat and mass transfer in complex three-dimensional geometries', *Publication 91/14 ISSN 1101–9972*, Dept. of Thermo- and Fluid Dynamics, Chalmers University of Technology, Göteborg, Sweden, 1991.
18. B. E. Launder, G. J. Reece and W. Rodi, 'Progress in the development of a Reynolds-stress turbulence closure', *J. Fluid Mech.*, **68**, 537–566 (1975).
19. F. S. Lein and M. A. Leschziner, 'Second-moment modelling of recirculating flow with a non-orthogonal collocated finite-volume algorithm', *Proc. 8th Symp. Turbulent Shear Flows*, Technical University of Munich, 1991, pp. 20.5.1–20.5.3.
20. B. Van Leer, 'Towards the ultimate conservative-difference-scheme. II. Monotonocity and conservation combined in a second-order scheme', *J. Comput. Phys.*, **14**, 361–370 (1974).
21. B. P. Leonard, 'A stable and accurate convective modeling based on quadratic upstream interpolation', *Comput. methods appl. mech. eng.*, **19**, 59 (1979).
22. F. Durst and F. Schmitt, 'Experimental studies of high Reynolds number backward-facing step flows', *Proc. 5th Symp. Turbulent Shear Flows*, Cornell University, 1985, pp. 5.19–5.24.
23. M. D. Deshpande and D. P. Giddens, 'Turbulence measurements in a constricted tube', *J. Fluid Mech.*, **97**, 65–89 (1980).
24. R. L. Simpson, 'Turbulent boundary-layer separation', *Ann. Rev. Fluid Mech.*, **21**, 205–234 (1989).
25. B. E. Thompson and J. H. Whitelaw, 'Characteristics of a trailing-edge flow with turbulent boundary-layer separation', *J. Fluid Mech.*, **157**, 305–326 (1985).